Pore network simulations coupled with innovative wettability anchoring experiment to predict relative permeability of a mixed-wet rock

Mohamed Regaieg[1*], *Franck* Nono[2], *Titly* Farhana Faisal[3], *Clément* Varloteaux[4] and *Richard* Rivenq[1]

[1] TotalEnergies SE
[2] Modis
3 Inria
[4] Computational Hydrocarbon Laboratory for Optimized Energy Efficiency

Abstract. Since the pioneering work of Oren et al. [1] several attempts have been made to predict relative permeability curves with Digital Rock Physics (DRP) technique. However, the problem has proved more complex than what researchers have expected, and these attempts failed. One of the main issues was the high number of uncertain parameters especially for the wettability input and this gets worst in mixed-wet scenario as the number of parameters is higher than in water-wet and oil-wet cases. In fact, Sorbie and Skauge stated that wettability assignment is the most complex and least validated stage in DRP simulation workflow. Similarly, Bondino et al. [2] concluded that "genuine prediction" of multi-phase flow properties will remain not credible until important progress is achieved in the area of wettability characterization at the pore scale.

In this work, we propose a pragmatic approach to tackle this problem. First, we develop an innovative fast anchoring experiment imaged by microCT scanner, that helps to determine several wettability parameters needed for the DRP simulation (including the fraction of oil-wet /water-wet pores, any spatial or radius correlation of oil wet pores …). This experiment also provides an estimation of residual oil saturation that is an important parameter and helps to anchor the pore scale simulations and further reduce the uncertainty. In addition to help reducing the uncertainty of the simulation, this experiment provides a fast (compared to Amott Harvey test) estimation of the wettability of the system. Images representing large volumes with low resolution are, first, improved with Enhanced Super Resolution Generative Adversarial Networks (ESRGAN) to obtain a large image with high resolution. Then, a pore network is extracted, and TotalEnergies parallel pore network simulator is used for multiphase flow simulations considering the constraints from the anchoring experiment to reduce the uncertainty. Finally, we compare our simulations against high quality SCAL experiment performed in-house and we assess the predictive power of our DRP workflow.

1- Introduction

Wettability input is key for DRP simulation as it controls the capillary forces and hence the invasion order. Unfortunately, it is not easy to characterize, and things become more complicated in mixed-wet scenario where fraction of oil-wet, water-wet, the spatial distribution of oil-wet pores and their correlation to the radii of the pores are important parameters needed to be indicated to the model. If one fails to do so, the model would have too many degrees of freedom and genuine predictions are not easy to achieve. In fact, [3] have stated that wettability assignment is the most complex and least validated stage in DRP simulation workflow. Similarly, [2] have concluded that "genuine prediction" of multi-phase flow properties will remain not credible until important progress is achieved in the area of wettability characterization at the pore scale.

Contact angle measurements from Micro-CT images of multiphase flow experiment has been very attractive recently [4]. However, as these measurements use the 3-phase contact line for the computations, they are very sensitive to the image resolution and insufficient image resolution leads to contact angle values close to 90 degrees with very large standard deviation [5]. Furthermore, automated contact angle measurements take into consideration the pinned menisci which are different from the contact angle input needed by a PNM simulator.

Recent observations [6,7] showed that wettability is correlated in space, and the pores having similar wettabilities are likely to be at a close spatial location. However, verifying that this correlation exists for a particular system and measuring the correlation length is not straightforward, requires one to perform a multiphase flow experiment and have several menisci in

* Corresponding author: mohamed.regaieg@totalenergies.com

neighboring pores which is not always easy to achieve. Then, image processing is needed in order to quantify the correlation length [7] which is not ideal for an industrial workflow.

Dixit et al. [8] proposed that wettability could be correlated to the size of the pores and proposed three models: Fractional-Wet model (i.e. contact angles are not correlated to the size of the pores), Mixed-Wet Large (i.e. where large pores are oil wet and small pores are water-wet) and Mixed-Wet Small (i.e. small pores are oil-wet and large pores are water-wet). They used this theory and PNM simulations to better interpret the differences between Amott-Harvey and USBM indices and proposed that the differences between these indicators could give an indication of the type of the wettability model.

[9] have demonstrated that fractional wet, mixed-wet large and mixed-wet small models are all possible theoretically. They also acquired Scanning Electron Microscopy (SEM) and Environmental Scanning Electron Microscopy (ESEM) images used to analyze mineralogy and local wetting properties. The ESEM used condensation of water to visualize if water appeared as drops on the surface (less water-wet), or as a water film condensed on the surface (water-wet). The water film was seen as whitening of the edges of the solid surface due to refraction of the water films. They also mentioned that they needed to analyze many images to be conclusive. Again, this is not practical in an industrial workflow where we aim to have a fast wettability characterization and feed it to a DRP model to be able to predict relative permeability curves quickly.

To solve the issues described above, we propose an innovative DRP simulation anchoring fast experiment that is easy to implement in an industrial workflow. It allows us to characterize the wettability of the sample, the fractions of OW and WW pores, determine the type of the wettability correlation to the radius of the pores, if there is any, and finally identifies if there is a wettability spatial correlation and allows the computation of this correlation length.

In this paper, we first describe TotalEnergies's DRP workflow based on 1) ESRGAN method to enhance the resolution of an image with a large field of view 2) GNM technique to extract a pore network with conductivities computed on the rock image, 3) a network stitching code that allows the extraction of large networks and 4) TotalEnergies' fully parallelized inhouse tool DynaPNM that can simulate flow in networks with several million pore elements.

Subsequently we describe and present the results of our wettability anchoring experiment that allows us to find the simulation wettability input as well as measure experimental parameters, such as S_{or} and $K_{rw}at\ S_{or}$ that allow us to constrain our simulations.

Then, we present the sensitivity study where the uncertain simulation parameters are varied and only the realisations in agreement with the wettability anchoring experiment results are kept. Hundreds of different realizations are used to produce P10, P50 and P90 relative permeability sets.

Finally, the simulated relative permeability curves are compared to an in-house SCAL experiment to assess the predictive potential of our simulation workflow.

2- Description of the simulation workflow

2.1. Enhanced Super resolution Generative Adversarial Networks (ESRGAN)

Acquiring micro-CT images of a rock is the first step in DRP simulation. This is then followed by segmenting the images to distinguish the rock from the pore space, and finally flow simulations are performed to compute advanced rock properties such as relative permeability and capillary pressure. [10] have proved that when the geometry of the pore space is well characterized, the flow simulators perform well.

However, the geometry of a real rock is not always well characterized, notably due to the lack of image resolution which in turn introduces uncertainty in the pore/throat geometry and consequently introduces errors in rock properties computation. Furthermore, during image acquisition a compromise is often made between the speed of the image acquisition, the size of the scanned volume and the resolution obtained: generally, increasing the resolution decreases the field of view, in turn limiting the quantity of information obtained from the image and thus making DRP simulations less representative.

In this work, we have implemented the ESRGAN method proposed by Wang et al. [11] . This method is based on two phases of training: PSNR step where the L1 loss function is minimized during the training of the generator. In this stage, the borders of the pores are improved but the texture of the rock is not captured. The weights of the trained generator are used as the starting point of the second stage of the training that we call GAN training. Pretraining with PSNR helps the GAN to have more visually pleasant results. The loss function of the second stage has three terms: the adversarial loss, the perceptual loss and the content loss. For the adversarial loss, Wang et al [11] proposed to use a relativistic average GAN [12] where loss function does not optimize discriminator to distinguish data real or fake. Instead, RaGAN's discriminator distinguishes that "real data isn't like average fake data" or "fake data isn't like average real data". According to Wang et al [11], this helps to learn sharper edges and more detailed textures. The perceptual loss helps the network to

capture perceptually relevant differences like textures or the clays in the rock images. These are determined from features maps obtained from VGG19 before the activation. We do not use the weights of the pre-trained VGG19 network, instead we re-train it with rock micro-CT images in order to have more relevant features and we have observed an improvement of the results after that. Finally, the content loss is the L1 pixel-by-pixel between the generated and the high-resolution images.

The loss for the generator is therefore

$$L_G = L_{percep} + \lambda L_G^{Ra} + \eta L_1$$

where L_{percep} is the perceptual loss, L_1 is the 1-norm distance between recovered image G(xi) and the ground-truth y, and λ (equal to 5 x 10^{-3}), η (equal to 1 x 10^{-2}) are the coefficients to balance different loss terms.

We have made the training parallel using multiple nodes and multiple GPUs in each node. The training is performed using two scans of the same small volume (1.45 microns image and 5.8 microns image), 3000 crops of 384*384 pixels images are made to form the training dataset. Training was performed using 36 GPUs and took 2 days. Afterwards, the trained model was applied to a second full low-resolution dataset of Bentheimer from another acquisition. An up-sampling in the Z direction was done on the low-resolution image that was next passed to the trained neural network. The generator was applied slice by slice on 2D images with 796 x 820 pixels to generate a 3D image of 3184 x 3280 x 12928 with voxel size of 1.45 microns. Then, we consider a subset from super resolution image, and we compare it to a high-resolution zoom of the same volume. Very good agreement was obtained when compared super resolution to high resolution images visually (**Fig *2***). **Fig 3** presents permeability and porosity computations for low resolution, high resolution and super resolution images for an ensemble of realistic segmentations.

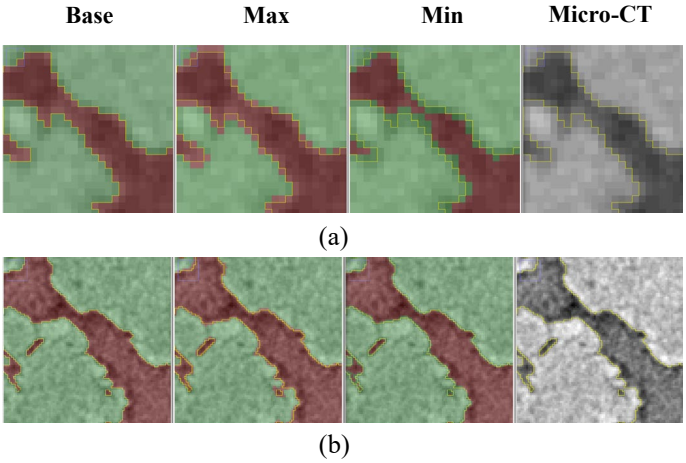

(a)

(b)

Fig 1 : Example of the several segmentation hypotheses considered in this work for a low-resolution image (a) and a high resolution image (b)

As segmenting the images could bias the results, we propose to perform for each image three realistic segmentations that a user is likely to consider. We choose a 'Min' segmentation with slightly underestimating the pore space comparing to the other segmentations, a 'Max' segmentation where pores are larger and a 'Base' segmentation between the 'Min' and 'Max' cases. We use machine learning based trainable Weka segmentation [13] where several classifiers are trained according to the scenarios defined above **Fig 1**

We observe that permeability and porosity computations are closer and have less uncertainty with super resolution. Next, we check the bodies and throat sizes distributions for high resolution, low resolution, and super resolution images. We clearly observe that the estimation of pore and throat radii is considerably improved with super resolution (**Fig 4**). **Fig 5** presents simulated capillary pressure curves using low resolution, high resolution and super resolution images. We note we have tried to use several realistic segmentations for each case to illustrate the uncertainty related to this step and therefore we present envelopes of capillary pressure curves. We can clearly notice that ESRGAN makes our simulated primary drainage capillary pressure curves more accurate. Having validated the ESRGAN approach we propose to use it in the next part of the paper. However, these large images are challenging to handle in DRP simulation, and we expose in the next sections our strategy to enable using them in our numerical study.

(a)

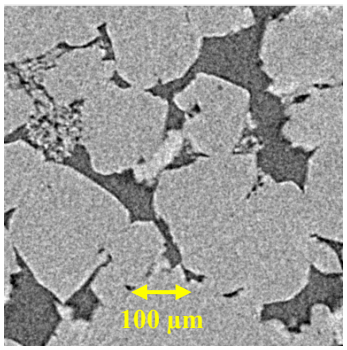

(b)

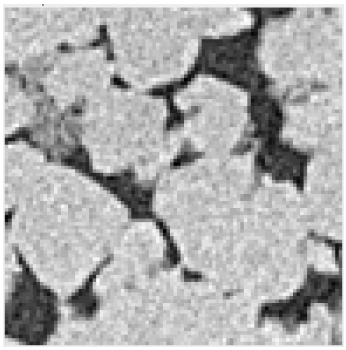

(c)

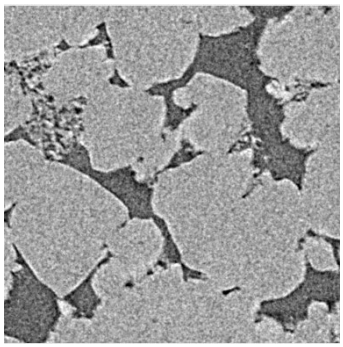

Fig 2 : comparison between super resolution (a), low resolution (b) and high resolution (c) images

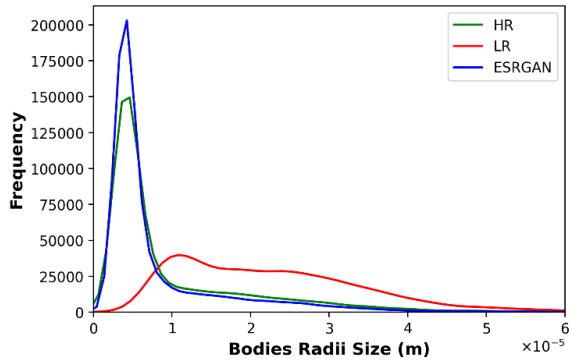

(a)

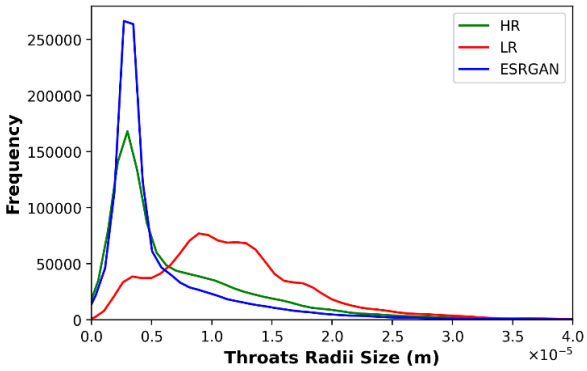

(b)

Fig 4 : Comparison between pore size distribution for bodies using Maximum Ball Algorithm (a) and throats (b) using 3 images: low resolution (red), super resolution (blue) and high resolution (green)

(a)

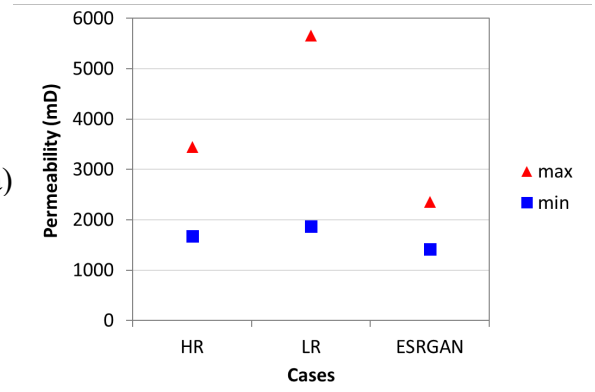

(b)

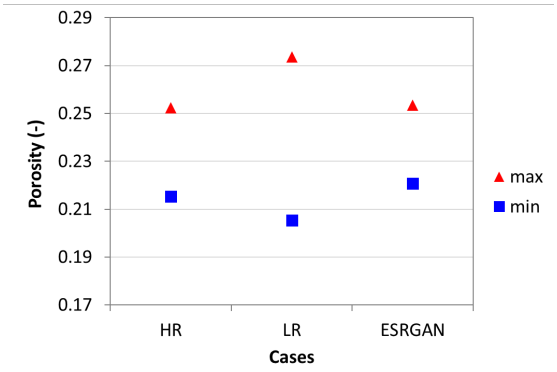

Fig 3 : Comparison of permeability using Openfoam (a) and porosity (b) for low, high and super resolution images for several realistic segmentations (max and min segmentation for each case)

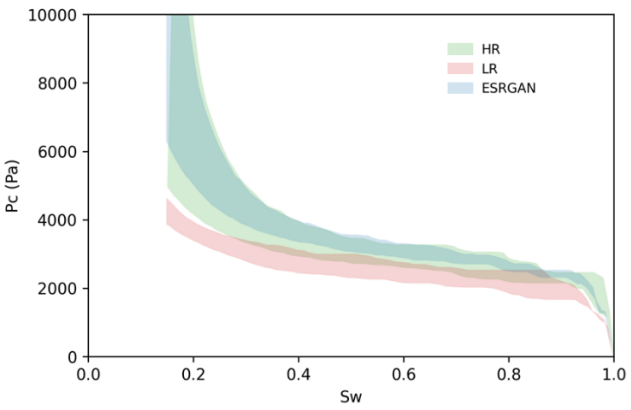

Fig 5 :Comparison between computed capillary pressure curves with TotalEnergies DRP simulation tools and using 3 images with several realistic segmentation: low resolution (red), super resolution (blue) and high resolution (green)

2.2. Pore Network Extraction

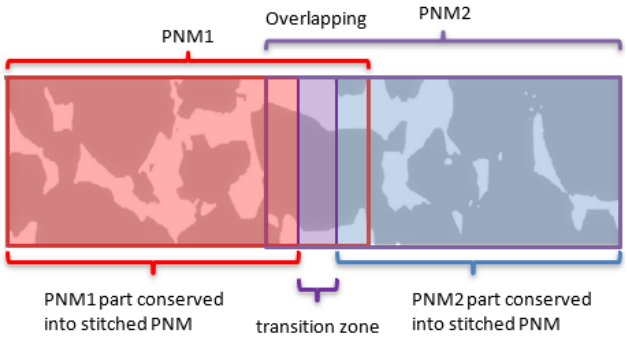

Fig 6 : An illustration of the pore network stitching process

In contrast to some digital rock physics methods, pore network models do not involve two-phase direct flow simulation in a 3D digital rock. Instead, it needs a pore network that is extracted from 3D reconstructions. Various algorithms exist to extract the skeleton of the 3D model that carries the essential geometric and topological information of the underlying pore system. In this work, we use a pore network extraction platform called GNextract developed with Imperial College, London [14] . GNextract is first used to reconstruct an upscaled version of the 3D segmented image of a rock in the form of a network of pore elements where the single-phase flow conductances in each pore are derived by solving the Stokes equation in the original geometry using OpenFOAM. Unfortunately, the extraction code needs a large amount of memory to extract large images (more than 60 GB of RAM for 1500^3 voxels image). Therefore, to overcome this limitation, a stitching process has been developed on networks extracted from overlapped sub-volume of a given image. Error! Reference source not found. illustrates the stitching process and shows that the stitched network is formed by a first part conserved from PNM1, a second part conserved from PNM2, and a third part obtained on a transition zone where rules inspired from the ones used by GNextract are defined to choose the elements. More details of the stitching process could be found in [15].

2.3. Pore network flow simulator

Once a pore network is extracted with the corresponding conductance values from single phase DNS simulation, we go on to perform two-phase flow simulations. These simulations are performed using DynaPNM, TotalEnergies' inhouse pore network simulator [16], that we use in quasi-static mode as all the cases that we study in this paper are capillary dominated.

The physical rules implemented in the simulator are broadly similar to the ones used in [1,17] with the exception of a major change in the film flow model [15]. The geometry of the pore network is simplified into an ensemble of pore bodies connected through pore throats during the pore network extraction step. As the invasions are totally controlled by the geometry, there is no need to compute the pressure gradients. The invasion order is determined through the capillary entry pressure of each element and the trapping is determined through a clustering algorithm. For every relative permeability point computation, the phases are isolated, and a pressure gradient is applied to the network. The pressure on each node is calculated, the corresponding production rate at the outlet is computed, and effective permeability of each phase is determined through Darcy's law.

The network is initially filled with water. A primary drainage is first simulated to establish irreducible water saturation, Swi. As the network is assumed water-wet, oil injection follows an invasion percolation regime. Water layers in pore elements with corners make water trapping very difficult and allow to achieve very low Swi values.

Primary drainage is then followed with a waterflood after an aging process where oil filled pore wettability is changed. First, water spontaneously fills the water-wet part of the network through piston like displacement and snap-off. In this phase the smallest pores are filled first, then the next smallest are filled, and so on. The defending oil phase can escape by flowing through oil-filled pores. Once spontaneous imbibition ends, the invading water is over pressured by applying a negative capillary pressure. Now, the largest pore elements are filled first, and oil can escape to the outlet either by flowing through the center of oil filled pores or through oil films. Once all the oil is trapped, the simulation stops.

The simulator has been parallelized to allow the simulation of large systems. First, the domain is decomposed, each processor has allocated memory and performs the computations of a subdomain. Each processor also needs information from the neighboring subdomains. The pore bodies and throats inside each subdomain of a processor are named local elements while the pore bodies and throats from neighbor subdomains are named ghost elements. Synchronization of the information of the ghost elements is performed after each capillary pressure step or after a maximum change in the network phases saturations. This communication is made using Message Passing Interface library MPI [18]. Furthermore, a parallel clustering algorithm has been implemented in order to determine if the defending phase is trapped and parallel linear solver library [19] is used for permeability and relative permeability computations. This parallelization allows us to simulate large networks with tens of million elements in few hours [15] .

2.4. Statistical analysis

Several input parameters of pore network simulation are uncertain, especially the ones linked to the wettability input. These uncertainties have been used by some researchers in the past to "tune" the simulation results to SCAL relative permeability curves. However, if one wants to be predictive, she/he should not know the result *a priori* and this makes choosing the uncertain parameters tricky. Therefore, we have designed a wettability anchoring experiment (described in the next section) to help us better estimate these wettability parameters. Subsequently, we have developed a statistical uncertainty workflow [15] in which we vary the uncertain pore network simulation parameters within the ranges determined from the experiment. First, thousands of DynaPNM input files are generated in an experimental design phase using WSP method [20]. Subsequently, flow simulations are run on TotalEnergies' supercomputer PANGEA. Then, a selection exercise is performed on these realisations to only keep the ones in agreement with S_{or} and K_{rw} at R_{os} measured from the wettability anchoring experiment. This is followed by a simulation ranking exercise based on the oil production after a given amount of water injected corresponding to each Kr curve and allows us to define three scenarios:

- P10: an optimistic scenario in which only 10% of the simulations produce more than this case
- P50: a median scenario in which 50% of simulations produce more than this case
- P90: a pessimistic scenario in which 90% of the simulations produce more than this case

3- Wettability anchoring experiment

Wettability is one of the main inputs of PNM simulation and unfortunately it is difficult to characterize *a-priori*. Moreover, even if a qualitative assignment of wettability is done and water-wet, oil-wet, or mixed-wet scenario is identified, a high number of uncertain parameters remains especially for mixed-wet case as the contact angles, the fractions of OW and WW pores, wettability spatial correlation and wettability correlations to pore radii (i.e., Do we have MWS, MWL or FW model) are all important parameters that could impact the simulation results. Considering all the possible values of these simulation inputs results in large simulation uncertainty which is not satisfactory.

Besides, performing a classical wettability test like the Amott Harvey or USBM needs a lot of time and does not provide all the information needed by the simulation.

Therefore, we have designed a fast wettability anchoring experiment imaged by micro-CT scanner that provides us with crucial data for our wettability input as well as some measurements that will help us constrain our simulation and thus reduce the uncertainty. We first test this approach on a Bentheimer sample as described in the next section.

3.1. Description of the experiment

We start our experiment by mounting a 6 mm diameter Bentheimer sample in a flow cell with confining pressure of 50 Bars, the experimental set-up is illustrated in **Fig 7**. First, we establish Swi using viscous displacement using mineral oil (Marcol52) where the same conditions (e.g., capillary number, same fluids …) are used comparing to the validation SCAL experiment described in the next section. This is followed by replacing the mineral oil with toluene then with dead crude oil and aging the sample for 2 weeks at 80° C in a similar protocol (e.g. injected pore volumes, rate, …) used by the SCAL laboratory. After the aging, Kro(Swi) was measured and a decrease of 30% of the Kro was obtained. This was followed by injection of 2.5 Pore volumes of decaline to remove the dead oil without impacting the actual plug's wettability. Next, mineral oil (Marcol52) was injected to replace decaline. We note that fluids replacement was performed at low flow rates to ensure that we do not change the initial water saturation. An image acquisition is performed after aging at Swi and this is followed by the start of a spontaneous imbibition phase. We use one end opened protocol where water enters the sample and oil leaves it from the same side in counter-current imbibition process. Very low capillary number (8E-09) was used for the leaching process that aims to remove the produced oil from the diffuser without forcing the flow of water into the sample.

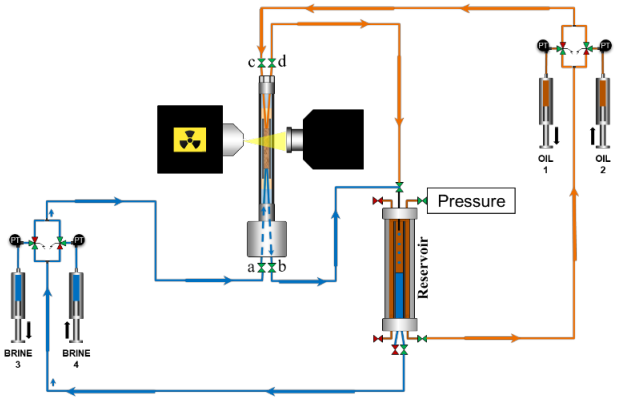

Fig 7 : Experimental set-up of the wettability anchoring experiment. In spontaneous imbibition c and d are closed, a and b are opened. In spontaneous drainage a and b are closed, c and d opened.

We only perform the spontaneous imbibition process for a week as we have observed that it was sufficient for water to imbibe in the first part of the sample to have a

fast experiment, but if time permits it can be interesting to continue the process for a longer time. Then, water is injected into the sample in a forced imbibition with the same maximum capillary number used in our SCAL lab. Finally, using a similar protocol we perform a spontaneous drainage in the other face of the sample. Micro-CT acquisitions are made at the end of each phase of the experiment.

The main objective of this test is to identify water-wet and oil-wet pores. It is obvious that water would imbibe to the water-wet pores in spontaneous waterflood and to the oil-wet pores in spontaneous drainage. This helps to map these pores and as a consequence analyze the volumes imbibed, the spatial correlation of wettability and the wettability correlations to the radii of the pores.

3.2. Analysis of the results

3.2.1- Wettability characterization and quantification of OW fraction

Fig 8 shows that water has imbibed during spontaneous imbibition and the comparison between the Swi image and the image at the end of spontaneous imbibition clearly shows some of the water-wet pores. Similarly, **Fig 9** shows that oil has imbibed during spontaneous drainage and the comparison shows some of the oil-wet pores. We point out here the water/oil have only access to the connected water-wet/oil-wet pores and that we did stop the spontaneous imbibition/drainage phase on purpose after a week as discussed previously.

Water has imbibed until the middle of our sample during spontaneous imbibition and oil entered to a length of 800 slices during the spontaneous drainage. In order to have a consistent analysis and to compare the imbibed volumes, we perform our analysis on the first 800 slices of the sample (i.e. from inlet side in spontaneous imbibition and from outlet side in spontaneous drainage) as we would like to compare the imbibed volumes.

We observed that in the first 800 slices of the sample the water saturation increased by 7.5%. Similarly, we observed that the oil saturation has increased by 2.3% on the same length from the outlet side. This confirms that we have a mixed-wet sample. However, it can be misleading as oil advances in spontaneous drainage meaning that receding contact angles will be the effective angles in this process. We may have a situation where a pore has an oil-wet advancing contact angle but a lower than 90° receding contact angle. These would not be accounted for in the imbibed oil volume. Furthermore, oil has not access to the already oil-filled pores at Sor that could be oil-wet. The analysis of the imbibed volumes demonstrates that the system is mixed-wet but we cannot yet compute the oil-wet fraction in the system.

(a)

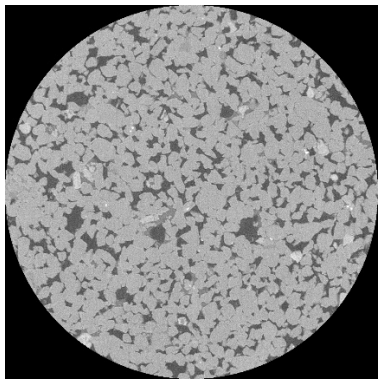

(b)

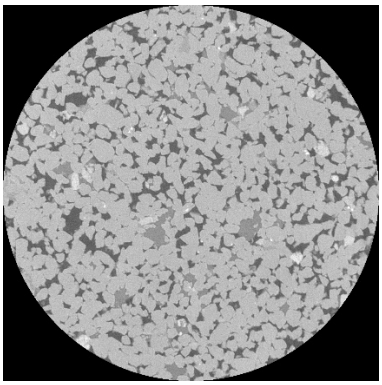

(c)

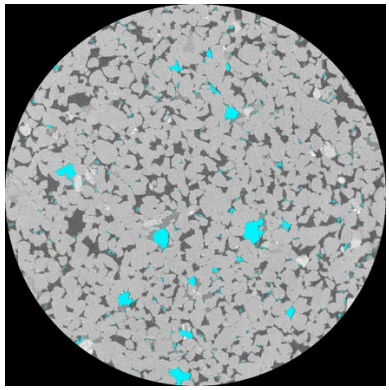

Fig 8 : Image of a slice from the experiment at Swi (a), after spontaneous imbibition (b) and the image after spontaneous imbibition with some water-wet pores highlighted in blue (c)

(a)

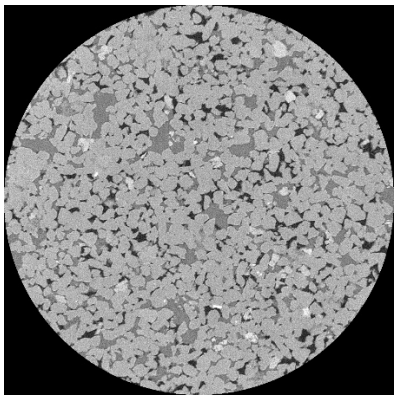

(b)

(c)

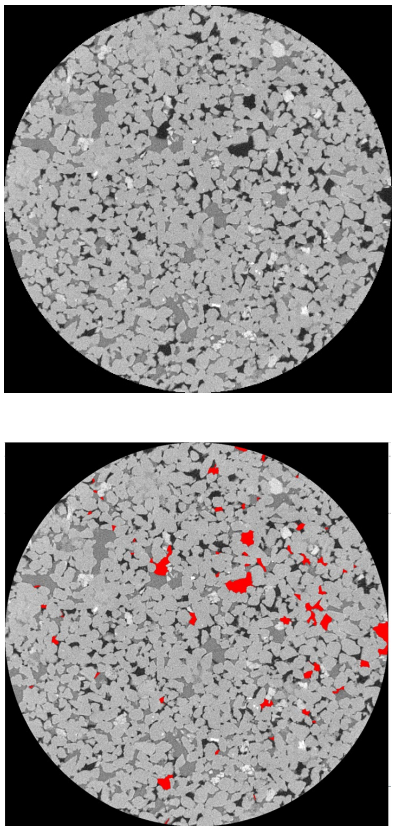

Fig 9 : Image of a slice from the experiment at Sor (a), after spontaneous drainage (b) and the image after spontaneous drainage with some oil-wet pores highlighted in red (c)

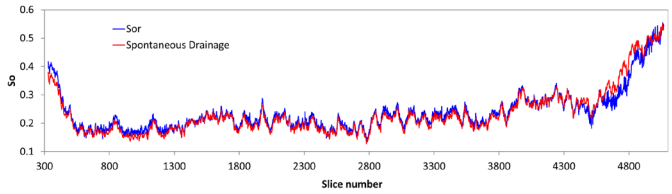

Fig 10 : Oil saturation profile at Sor (blue) and after spontaneous drainage (red). Injection performed from left to right.

The saturation profile of the oil at Sor **Fig 10** shows a capillary end effect which is an indication that the system is not water-wet. Furthermore, this provides us with important information about the oil saturation at Pc equal to zero that was 55%. This helps us to characterize the oil-wet fraction in the system that is needed to achieve this. We estimate it to 53-63% of oil-wet fraction after a fast PNM sensitivities study where the Pc=0 was reached at Sw~0.45. We also note that by considering the oil profile at the center we are able to estimate the residual oil saturation that we use in the selection exercise later. Moreover, we have measured the Krw at ROS in this experiment that should be close to Krw at Sor. We then add an uncertainty to this measurement and use it as a constraint in the selection exercise described later.

Finally, the fact that the imbibed water volume was much higher than the imbibed oil volume for the same duration and at the same sample length gives us an indication that the receding contact angle was lower than 90° in a considerable amount of the oil-wet pores. This is an interesting information that we keep in mind when we choose the oil-wet contact angles input of the simulation.

3.2.2- Wettability correlation to the radii of the pores

As discussed previously, [7] proposed that wettability could be correlated to the size of the pores and proposed 3 models: Fractional-Wet model (i.e. contact angles are not correlated to the size of the pores), Mixed-Wet Large (i.e., where large pores are oil wet and small pores are water-wet) and Mixed-Wet Small (i.e., small pores are oil-wet and large pores are water-wet). Identifying the wettability model (i.e. FW, MWS or MWL) is important for PNM simulation as it impacts the invaded pores and the residual oil saturation [9] . Oil that imbibes into the system in spontaneous drainage does not have access to the full rock as a part of the porosity is already filled with oil. Therefore, we propose to perform this analysis on the water-wet pores that had access to all the pore space during the spontaneous imbibition.

A pore network has been extracted from the images and used to analyze the experimental results. **Fig 11** presents the pore radii distribution of the water-wet pores and **Fig 12** shows the volumetric fraction of water-wet pores as a function of the pore radii. We can observe a clear correlation between the pore radius and the percentage of water-wet pores in the system that demonstrates that for this system large pores are more likely to be water-wet. We conclude then that we are in a MWS wettability model.

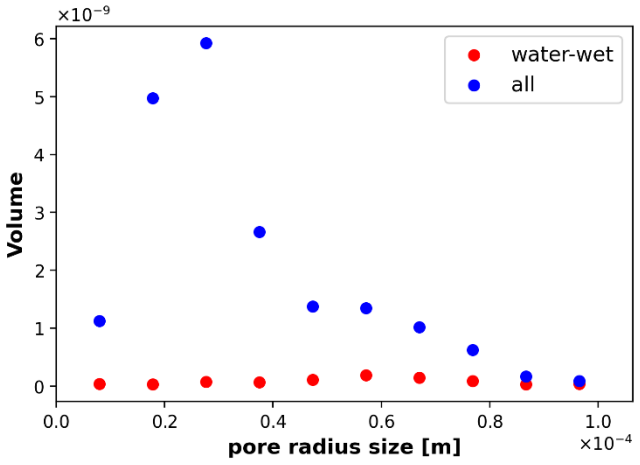

Fig 11 : The pore radii distribution obtained after extracting a pore network (blue) and the water-wet pore size distribution obtained from analyzing the pores occupancy (red)

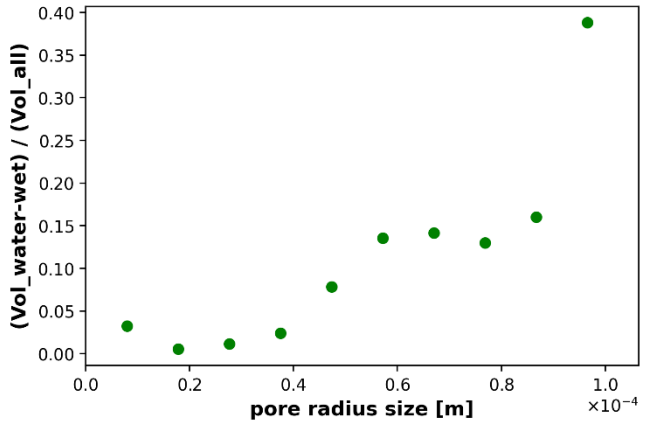

Fig 12 : The water-wet volumetric fraction as a function of the pore radius obtained after extracting a pore network and analyzing the fluids occupancies

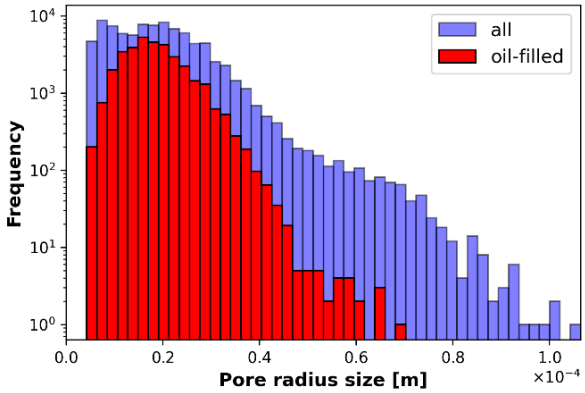

Fig 13 : Radii of oil filled pores at residual oil saturation, oil remains in the small pores

Fig 13 shows the oil filled pores at residual oil saturation, we observe that oil remains in the small pores which is what we expect in a MWS scenario as during waterflood water will first invade the water-wet pores then the larger oil-wet pores as the fluids will enter first the pores with lower capillary entry pressure in a drainage process [9]. This makes us more confident in the results of our analysis.

3.2.3- Spatial correlation of wettability

In this section, we investigate whether the wettability is correlated in space with clumps of more oil-wet and water-wet pores. This is an important parameter for the simulation and could have significant implications of the phase's connectivity especially through the flow in layers which would impact the relative permeability curves and the residual oil saturation. We propose to analyze spatial correlation using the water-wet pore's location determined from the extracted pore network because water had access to the full pore space during the spontaneous imbibition as explained in the previous section.

A common way of visualizing the spatial autocorrelation of a variable is a variogram plot (**Fig *14***) The correlation length can be regarded as a measure for the stationarity of a specific parameter distribution in space. In this case, the semi variance becomes stationary at a correlation length of 500 µm that represents for this rock 6 node to node lengths. This could be an important parameters for the simulations and in some cases it is not possible to match experimental observations if spatial correlation is not quantified properly [6]

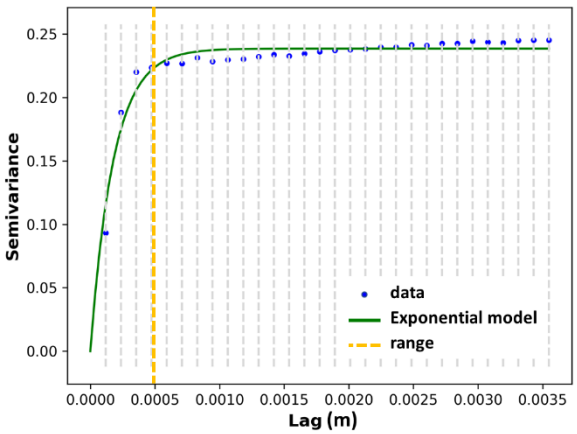

Fig 14 : Variogram plot for the water-wet pores using scikit-gstat [21]. It shows a correlation length of 500 µm

To summarize, the wettability experiment provides us with:

1- The fractions of oil-wet and water-wet pores obtained from the analysis of the capillary end effect
2- An indication of the contact angles in the oil-wet pores from the comparison of the volumes imbibed during spontaneous waterflood and spontaneous imbibition. For instance, if there is 50% oil-wet pores but nothing imbibes in spontaneous drainage it means that advancing contact angles are higher than 90° and receding contact angles are lower than 90°. Then, when we choose our contact angles we will select angles not too far from 90°. Similarly, if we have 50% oil-wet pores and similar volumes imbibed in the spontaneous imbibition and spontaneous drainage this means that even the receding contact angle in all pores is still higher than 90° then we know that we need higher contact angles in the oil-wet part.
3- The mapping of the water-wet pores provides us with a computation of the spatial correlation length
4- The mapping of the water-wet pores provides us with information of the wettability correlation to the pore radii (i.e.: MWS, MWL or FW)

4- Validation of DRP simulation workflow

Having built the DRP workflow, we proceeded to its validation. First, we took a low-resolution Bentheimer image at 5.8 microns that we enhance using ESRGAN to improve its resolution by a factor 4 and obtain an image with 3184x3280x12928 voxels. This image has the same aspect ratio as the SCAL experiment described below to avoid any differences created by different aspect ratios. Then, a stitching process was applied on the super-resolution image described previously. The image was divided into several subvolumes (2*2*9 along X, Y and Z) and networks were extracted from each sub-volume and stitched together. A network with 3.6 million elements was generated. After that, we create our experimental design to vary the simulation parameters within the uncertainty ranges. The input of the wettability anchoring is key at this stage and allows us to reduce the ranges of our parameters and hence have a smaller dispersion in our simulation results. In our experimental design, 3000 realizations have been generated and simulated (with varying the seeds numbers, the parameters of the contact angle distributions as described in table 1 and wettability spatial correlation parameters…) and mixed-wet small wettability model has been used in all the simulations. More details of our simulation input parameters can be found in **Table 1** . We note that we have used two contact angle distributions: the first in the oil-wet part of the sample and the second in the water-wet pores. The choice of these pores was made to be consistent with a mixed-wet small wettability model and considering spatial auto-correlation of pores with similar wettability. The wettability anchoring experiment did not provide us with direct information about contact angles. However, it gave indirect information about the oil-wet contact angles. In fact, imbibed water volume was much higher than the imbibed oil volume for the same duration and at the same sample length gives us an indication that the receding contact angle was lower than 90° in a considerable amount of the oil-wet pores. Therefore, we chose medium to low oil-wet contact angles to be consistent with this observation.

Table 1 : Simulation parameters used in Mixed-Wet Bentheimer simulations

Parameters	Value/Range
PD receding contact angle distribution	Normal distribution
PD receding contact angle standard deviation	4°-8°
Mean receding PD distribution	20°-30°
WF dist1 (oil-wet) advancing contact angle distribution	Normal distribution
WF dist1 (oil-wet), advancing contact angle standard deviation	4°-8°
Mean advancing WF dist1 (oil-wet) contact angle	115°-135°
WF dist 2 (water-wet) advancing contact angle distribution	Normal distribution
WF dist2 (water-wet), advancing contact angle standard deviation	4°- 8°
Mean advancing WF dist2 (water-wet) contact angle	70°-89°
Fraction of distribution 2 (water-wet fraction)	0.37-0.47
Correlation length	5-7 pores
Wettability model	Mixed-Wet Small
Initial water saturation	0.12-0.13

We observed that after aging in the anchoring experiment, several water droplets appeared on the center of the pores (**Fig 15**). We think that these correspond to some water layers that got disconnected after aging and that fall in the center of the pores. We measured that the oil relative permeability decreased by 30% during the aging, we apply therefore this reduction by scaling our simulated oil relative permeability. This reduction of permeability would not impact the water relative permeability since pores are filled with a single phase after the water invades them during waterflood.

(a)

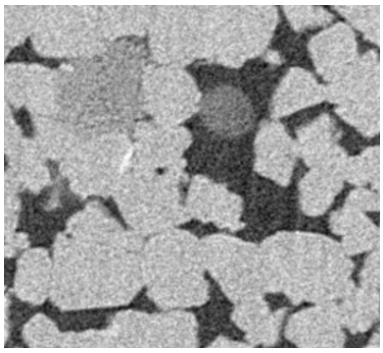

(b)

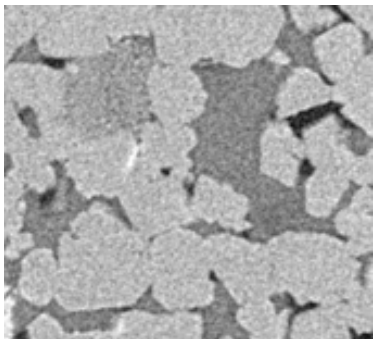

Fig 15 : Multiphase CT images at Swi after aging (a) and at Sor (b). It shows that water (dark grey) droplets were blocking an oil (black) filled pore at Swi and that the same pore becomes fully filled with water at the end of waterflood.

In order to reduce the uncertainty further, we use the measured parameters in the anchoring experiment and only keep the realizations that agree with the measurements from the wettability anchoring experiment. Therefore, we only keep simulations that have:

- Pc=0 between Sw=0.4 and Sw=0.5
- 0.1<Krw (Sor)<0.2
- 0.18<Sor<0.26

After performing our blind simulation test, we compare the results to a high quality unsteady-state experiment performed in-house. The SCAL experiment was performed on a 5 cm diameter Bentheimer plug with 20 cm length. The plug had a porosity of 24% with an absolute brine permeability of 2.3D. Primary drainage was achieved through oil flooding using a displacement with viscous oil to target a low S_{wi} exempted from capillary end-effect. A homogeneous S_{wi} profile of average 12.1% was obtained. To make the plug mixed-wet, the same dead oil used on the anchoring wettability experiment was used to replace the mineral oil and perform 15 days of dynamic ageing process at 80°C to alter wettability of the SCAL plug. Afterwards, multi-rates waterflood at 80°C was performed. Initial flow rates were sized to fit Hagoort criteria [22] to avoid viscous fingering. It started at around 0.3ft/day. Oil production-pressure gradient vs time, and transient to equilibrium saturation profiles through 2D X-ray imaging internal devices were acquired during the experiment and numerical interpretation was performed using the software CYDAR® to find the best couple (Kr/Pc) matching oil production, pressure gradient and saturation profiles (transient and equilibrium).

Fig 16 shows our simulated relative permeability curves with all realizations and the P10, P50 and P90 scenarios obtained after ranking the oil production after 1 pore volume injected. We observe that our curves were in very good agreement with SCAL relative permeability that was presented by an envelope to consider the associated uncertainty. In fact, in an unsteady-state relative permeability experiment, the production data are then inverted in order to determine relative permeability curves. This inversion is non-unique and therefore we represent the SCAL relative permeability curve with an envelope of possible inversions of production data. This makes us confident about the predictive potential of DRP simulation when well informed with experimental data.

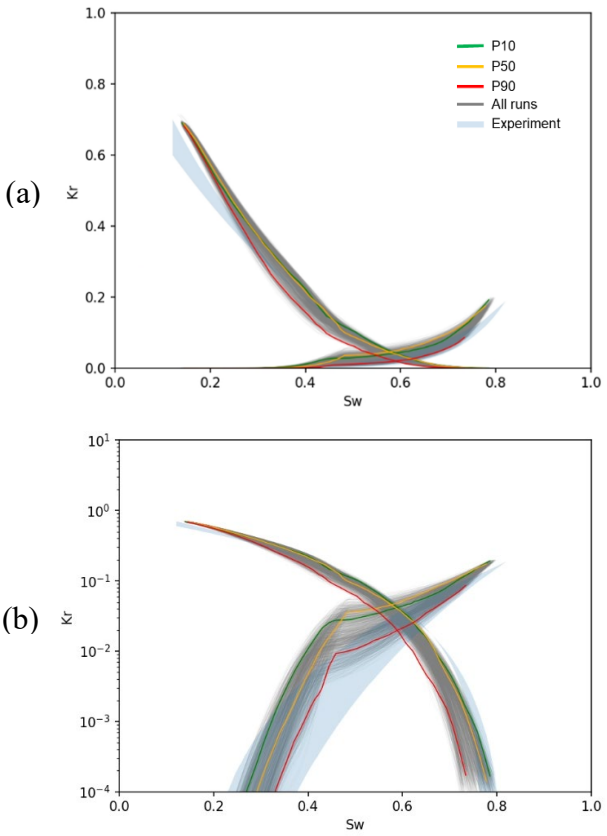

Fig 16 *:* Comparison between the simulated relative permeability curves: all realization (grey), P10 (green), P50 (yellow) and P90 (red) and experimental data (blue). We present the plots in linear (a) and log scales (b)

5- Conclusions

In this study we have applied TotalEnergies' DRP simulation workflow to predict the relative permeability in a Mixed-Wet Bentheimer. First, we augmented a low-resolution image using ESRGAN in order to have an image with a large field of view and fine resolution. Then, we extracted a pore network from this image using a stitching methodology.

Wettability input has been the weakest point of DRP simulation in the last few decades as it is difficult to quantify the values of contact angles, the wettability model and the spatial distribution of contact angles leading to having high number of degrees of freedom. Therefore, we have designed an innovative fast experiment that helps us to characterize wettability and have more reliable PNM simulations. With this experiment we could characterize that we have a mixed-wet system and identify the wettability model. In fact, we clearly observed that wettability in our sample was correlated to the radius and that the large pores were water-wet and the small oil-wet. The pore radii of the oil filled pores at residual oil saturation confirmed our observation as oil remained in the small pores which is a characteristic of mixed-wet small model. We could

also observe a spatial correlation of wettability and the correlation length had 6 pores length.

Having obtained all this information, we could run several hundreds of realizations of our simulations using our parallel PNM simulator where we varied the parameters within the identified uncertainty ranges. Furthermore, this experiment provided us with important measurements that helped us better constrain our simulations and we only kept the realizations that agreed with the measured data. Afterwards, our simulations were compared to a high quality in-house SCAL experiment performed with the same rock, same fluids and similar conditions. A very good agreement was obtained between the simulated and experimental data.

This study provided very promising results that, if confirmed by similar validation tests, would indicate that DRP simulation coupled with our pragmatic approach to characterize wettability is ready to be used in operational studies.

Acknowledgements

The authors would like to thank TotalEnergies management for the authorization to publish this work. Régis Brugidou is acknowledged for the fruitful discussions about the experimental set-up.

References

[1] Oren P-E, Bakke S, Arntzen OJ. Extending predictive capabilities to network models. SPE journal 1998;3(04):324–36.

[2] Bondino I, Hamon G, Kallel W, Kac D. Relative Permeabilities From Simulation in 3D Rock Models and Equivalent Pore Networks: Critical Review and Way Forward1. SPWLA-2012-v53n6a2 2013;54(06):538–46.

[3] Sorbie KS, Skauge A. Can Network Modeling Predict Two-Phase Flow Functions? SPWLA-2012-v53n6a2 2012;53(06):401–9.

[4] AlRatrout A, Raeini AQ, Bijeljic B, Blunt MJ. Automatic measurement of contact angle in pore-space images. Advances in Water Resources 2017;109:158–69.

[5] Sun C, McClure JE, Mostaghimi P, Herring AL, Meisenheimer DE, Wildenschild D, Berg S, Armstrong RT. Characterization of wetting using topological principles. J Colloid Interface Sci 2020;578:106–15.

[6] Foroughi S, Bijeljic B, Lin Q, Raeini AQ, Blunt MJ. Pore-by-pore modeling, analysis, and prediction of two-phase flow in mixed-wet rocks. Phys. Rev. E 2020;102(2):23302.

[7] AlRatrout A, Blunt MJ, Bijeljic B. Spatial correlation of contact angle and curvature in pore-space images. Water Resour. Res. 2018;54(9):6133–52.

[8] Dixit AB, Buckley JS, McDougall SR, Sorbie KS. Empirical measures of wettability in porous media and the relationship between them derived from pore-scale modelling. Transport in Porous Media 2000;40(1):27–54.

[9] Skauge A, Spildo K, Høiland L, Vik B. Theoretical and experimental evidence of different wettability classes. JOURNAL OF PETROLEUM SCIENCE AND ENGINEERING 2007;57(3-4):321–33.

[10] Yang J, Bondino I, Regaieg M, Moncorgé A. Pore to pore validation of pore network modelling against micromodel experiment results. Computational Geosciences 2017;21(5):849–62.

[11] Wang X, Yu K, Wu S, Gu J, Liu Y, Dong C, Qiao Y, Change Loy C. Esrgan: Enhanced super-resolution generative adversarial networks. In: Proceedings of the European conference on computer vision (ECCV) workshops. p. 0.

[12] Jolicoeur-Martineau A. The relativistic discriminator: a key element missing from standard GAN. arXiv preprint arXiv:1807.00734 2018.

[13] Arganda-Carreras I, Kaynig V, Rueden C, Eliceiri KW, Schindelin J, Cardona A, Sebastian Seung H. Trainable Weka Segmentation: a machine learning tool for microscopy pixel classification. Bioinformatics 2017;33(15):2424–6.

[14] Raeini AQ, Bijeljic B, Blunt MJ. Generalized network modeling: Network extraction as a coarse-scale discretization of the void space of porous media. Phys. Rev. E 2017;96(1):13312.

[15] Regaieg M, Bondino I, Varloteaux C, Farhana Faisal T, Yang J, Rivenq R (editors). Large two phase Digital Rock Physics simulations for relative permeability uncertainty assessment; 2021.

[16] Regaieg M, Moncorgé A. Adaptive dynamic/quasi-static pore network model for efficient multiphase flow simulation. Computational Geosciences 2017;21(4):795–806.

[17] Valvatne PH, Blunt MJ. Predictive pore-scale modeling of two-phase flow in mixed wet media. Water Resour. Res. 2004;40(7).

[18] Gropp W, Gropp WD, Lusk E, Lusk, Argonne Distinguished Fellow Emeritus Ewing, Skjellum A. Using MPI: portable parallel programming with the message-passing interface. MIT press; 1999.

[19] Balay S, Abhyankar S, Adams M, Brown J, Brune P, Buschelman K, Dalcin L, Dener A, Eijkhout V, Gropp W. PETSc users manual 2019.

[20] Sergent M. Contribution de la Méthodologie de la Recherche Expérimentale à l'élaboration de matrices uniformes: Application aux effets de solvants et de substituants. Aix-Marseille 3; 1989.

[21] Mälicke M. SciKit-GStat 1.0: a SciPy-flavored geostatistical variogram estimation toolbox written in Python. Geoscientific Model Development 2022;15(6):2505–32.

[22] Hagoort J. Displacement stability of water drives in water-wet connate-water-bearing reservoirs. Society of Petroleum Engineers Journal 1974;14(01):63–74.